Microporous and Mesoporous Materials 194 (2014) 8–14

Contents lists available at ScienceDirect

Microporous and Mesoporous Materials

journal homepage: www.elsevier.com/locate/micromeso

Synthesis of SAPO-34 with alkanolamines as novel templates and their application for CO_2 separation

Dehua Wang [a,b,c], Peng Tian [a,b], Miao Yang [a,b], Shutao Xu [a,b], Dong Fan [a,b,c], Xiong Su [a,b,c], Yue Yang [a,b], Chan Wang [a,b,c], Zhongmin Liu [a,b,*]

[a] National Engineering Laboratory for Methanol to Olefins, Dalian Institute of Chemical Physics, Chinese Academy of Sciences, P.O. Box 110, 116023 Dalian, PR China
[b] Dalian National Laboratory for Clean Energy, Dalian Institute of Chemical Physics, Chinese Academy of Sciences, Dalian, PR China
[c] Graduate University of Chinese Academy of Sciences, Beijing 100049, PR China

ARTICLE INFO

Article history:
Received 23 December 2013
Received in revised form 5 March 2014
Accepted 18 March 2014
Available online 28 March 2014

Keywords:
Molecular sieve
Aminothermal synthesis
SAPO-34
Alkanolamine
CO_2 adsorption

ABSTRACT

Alkanolamines are used for the first time as both the solvent and template to explore the syntheses of SAPO molecular sieves. Diglycolamine (DGA) and diisopropanolamine (DIPA) are found to act as novel structure-directing agent for the synthesis of SAPO-34, and N-methyldiethanolamine leads to the crystallization of SAPO-44. The obtained SAPO-34s are well characterized and investigated as adsorbents for selective separation of CO_2 from N_2 and CH_4. A close relationship between the acid concentration of SAPO-34 and CO_2 adsorption capacity has been revealed. SAPO-34-DGA with the highest acid concentration (sample D4) exhibits the best CO_2 adsorption capacity and high CO_2-over-N_2 selectivity. Breakthrough experiments are further carried out based on sample D4, which shows an excellent dynamic preferential adsorption ability for CO_2 (~8.2 wt%) from both CO_2/N_2 and CO_2/CH_4 mixtures (298 K). These results demonstrate that SAPO-34-DGA could be a promising adsorbent for the CO_2 capture.

1. Introduction

Molecular sieves are an important class of crystalline microporous inorganic materials, which have been widely applied in industry as catalysts, ion exchangers, and adsorbents [1–3]. For the past three decades, the development of molecular sieve synthesis has greatly extended their framework types and compositions, and more than 200 zeotype structures have been identified [4]. Any progress in the field of molecular sieves might promote motivate their innovative application and establish some new industrial processes. Therefore, it is always attractive to explore new zeotype materials and novel synthetic methodologies [5].

SAPO-34 molecular sieve, first reported by the scientists of Union Carbide Company in the 1980s [6,7], is one of the most important members in the silicoaluminophosphate molecular sieve family. It has exhibited excellent performance in the methanol-to-olefin (MTO) reaction [8,9] and good selective separation capacity for CO_2 from CH_4 or N_2 [10–12]. The synthesis of SAPO-34 could be fulfilled by many strategies, including hydrothermal method [6–12], solvothermal method [13,14], and dry-gel conversion [15]. Very recently, an interesting solvent-free synthesis method has also been developed by Xiao et al. [16]. Meanwhile, multiple templates have showed structure-directing ability to the synthesis of SAPO-34 such as tetraethylammonium hydroxide (TEAOH) [17], morpholine (MOR) [18], piperidine [19], dipropylamine [20], triethylamine (TEA) [21] and diethylamine (DEA) [22]. It is well acknowledged that SAPO-34 crystallized with different templates might leads to different morphology, microstructure, and Si coordination environment (acidic property), and thus differs in their catalytic properties. For example, TEAOH is capable to direct the synthesis of SAPO-34 nanocrystals with long lifetime and high selectivity to light olefins in the MTO reaction [17]. While both MOR and DEA tend to synthesize micro-sized SAPO-34 crystals with high Si incorporation into the framework [18,22]. These kinds of SAPO-34s generally exhibit shorter lifetime in the MTO reaction than SAPO-34 templated by TEAOH [17,22,23]. Barthomeuf et al. have made pioneering research about the relationship between template types and Si environments. They found that the templates in the cages of SAPO-34 were essential for the compensation of framework charges produced by the silicon incorporation accompanied by the generation of Brønsted acid sites via SM2 mechanism or SM2–SM3 combination. The template number per cage was mainly determined by the molecule size of organic amine, which had a great effect on the maximum concentration

* Corresponding author at: National Engineering Laboratory for Methanol to Olefins, Dalian Institute of Chemical Physics, Chinese Academy of Sciences, P.O. Box 110, 116023 Dalian, PR China. Tel./fax: +86 0411 84379289.
E-mail address: liuzm@dicp.ac.cn (Z. Liu).

http://dx.doi.org/10.1016/j.micromeso.2014.03.028
1387-1811/

of single Si environment in the framework. That is, the more amine molecules occluded in the cage, the higher single Si (4Al) concentration in the framework [24,25].

Nowadays, selective separation of CO_2 from gas streams is of paramount importance since its accumulation in environment can cause severe global warming [26,27]. Besides, the removal of CO_2 from CH_4 is an attractive issue in the processing of natural gas, because that the existence of CO_2 in natural gas will reduce the energy content and its acidity caused by water will lead to pipeline corrosion [28,29]. Currently, the technology based on absorption in aqueous solution of alkanolamines has been commercialized, but this method is very complex and produces corrosion for the equipment [30]. It is highly desirable to develop adsorption processes with porous materials as adsorbents, such as pressure swing adsorption (PSA), in which less energy consumed and no chemical solvents required. Compared with other nanoporous adsorbents, molecular sieves offer many advantages such as adjustable pore apertures, moderate surface polarity, and good thermal/hydrothermal stability. Many research works have been reported on the adsorption behaviors of zeolites A, X, Y, RHO, ZK-5, and chabazite etc. [31–36]. The adsorption properties of zeolites can be modified by changing the cations inside the channels or cages of zeolites [37,38]. In addition, SAPO molecular sieves also attract interests as CO_2 adsorbents. The electrostatic interaction of SAPO frameworks with CO_2 is generally weaker than that of zeolites, which may benefit the regeneration of adsorbents. Hedin once compared the water adsorption isotherms of SAPOs with that of zeolite 13X and claimed that SAPO molecular sieves are less moisture-sensitive than 13X, which is important to the practical application of SAPO adsorbents [39].

Among SAPO molecular sieves, SAPO-34 is one of the most intensively studied whatever in swing adsorption process or membrane separation [40,41]. The good properties of SAPO-34 in adsorption/separation are believed to be arising from its large pore volume and suitable pore diameter (0.38 nm), which is close to the kinetic diameter of CH_4 (0.38 nm) but larger than that of CO_2 (0.33 nm). Many methods such as extra-framework cation modification and amine functionalization have been explored to improve the CO_2 adsorption capacity or separation selectivity on SAPO-34 [42,43]. However, the influence of the acid properties of SAPO molecular sieves on the gas adsorption has draw less attention though acid sites of SAPO molecular sieves were evidenced to be the preferential adsorption sites for CO_2 [39,44]. An interaction between the acidic hydroxyl group and CO_2 ($H^+\cdots O(CO_2)$) has been proposed and rationalized by theoretical calculations [45].

Recently, a novel aminothermal synthesis method has been developed by our laboratory, where organic amines playing as both the solvent and template lead to the crystallization of SAPO molecular sieves with high yields and good properties [13,14]. Herein, alkanolamines, combining the properties of amine and alcohol [46], are used for the aminothermal synthesis of SAPO molecular sieves. Fortunately, several alkanolamines are found as novel templates to direct the structure of SAPO-34 and SAPO-44 molecular sieves. The obtained SAPO-34s with different Si contents are explored for CO_2 separation, and one of them shows excellent performance.

2. Experimental

2.1. Sample preparation

All alkanolamines used in the synthesis were analytically reagents. Silica sol (30.3 wt%), pseudoboehmite (72.5 wt%) and phosphoric acid (85 wt%) were used as inorganic reactants.

Eight kinds of alkanolamines, including triethanolamine (TEOA), diethanolamine (DEA), diisopropanolamine (DIPA), triisopropanolamine (TIPA), N,N-dimethylethanolamine (DMEA), N,N-diethylethanolamine(DEAE), N-methyldiethanolamine (MDEA), and diglycolamine (DGA), were tried to aminothermally synthesize of SAPO molecular sieves.

A typical synthesis procedure was as follows: alkanolamine, water, pseudoboehmite and silica sol were added in sequence into a glass beaker. The mixture was stirred at room temperature for 10 min, and then transferred into a stainless steel autoclave. Subsequently the phosphoric acid was added into the mixture drop by drop with stirring and a homogeneous and viscous mixture was obtained, following which the autoclave was sealed quickly and placed in an oven. After the autoclave being rotated at 50 rpm for 30 min to get a more homogeneous mixture, it was heated to 473 K within 90 min under rotation and kept for 48 h. At the end of the crystallization, the products were recovered by filtration with distilled water, and dried at 393 K in air. As-synthesized materials were calcined in air at 823 K for 2 h to obtain the template-free samples.

2.2. Characterizations

The powder XRD patterns were recorded on a PANalytical X′ Pert PRO X-ray diffractometer with Cu-Kα radiation (λ = 1.54059 Å), operating at 40 kV and 40 mA. The chemical composition of the samples was determined with Philips Magix-601 X-ray fluorescence (XRF) spectrometer. The crystal morphology was observed by field emission scanning electron microscopy (Hitachi, SU8020). All the solid state NMR experiments were performed on a Bruker AvanceIII 600 spectrometer equipped with a 14.1 T wide-bore magnet. The resonance frequencies were 600.13, 156.4, 242.9 and 119.2 MHz for ^{1}H, ^{27}Al, ^{31}P and ^{29}Si, respectively. ^{27}Al and ^{31}P MAS NMR experiments were performed on a 4 mm MAS probe with a spinning rate of 12 kHz. ^{27}Al MAS NMR spectra were recorded using one pulse sequence. A 200 scans were accumulated with a $\pi/8$ pulse width of 0.75 μs and a 2 s recycle delay. Chemical shifts were referenced to $(NH_4)Al(SO_4)_2{\cdot}2H_2O$ at −0.4 ppm. ^{31}P MAS NMR spectra were recorded using high-power proton decoupling. A 100 scans were accumulated with a $\pi/4$ pulse width of 2.25 μs and a 4 s recycle delay. Chemical shifts were referenced to 85% H_3PO_4 at 0 ppm. ^{29}Si MAS NMR spectra were recorded with a 7 mm MAS probe with a spinning rate of 6 kHz using high-power proton decoupling. A 5000–6000 scans were accumulated with a $\pi/4$ pulse width of 2.5 μs and a 10 s recycle delay. Chemical shifts were referenced to 4,4-dimethyl-4-silapentane sulfonate sodium salt (DSS). ^{1}H MAS NMR spectra were recorded using a 4 mm MAS probe. The pulse width was 2.2 μs for a $\pi/4$ pulse, and 32 scans were accumulated with a 4 s recycle delay. Samples were spun at 12 kHz, and chemical shifts were referenced to adamantane at 1.74 ppm. Before ^{1}H MAS NMR measurements, the samples were dehydrated typically at 693 K under pressure below 10^{-3} Pa for 20 h. The software Dmfit was employed for deconvolution using fitting of Gaussian–Lorentzian lineshapes. For the determination of quantitative results, all samples were weighed, and the spectra were calibrated by measuring a known amount of adamantine performed in the same conditions. N_2 adsorption–desorption isotherms were obtained on a Micrometrics ASAP 2020 system at 77 K. The total surface area was calculated based on the BET equation. The micropore volume and micropore surface area were evacuated using the *t*-plot method. The thermal analysis was performed on a TA Q-600 analyzer with a temperature-programmed rate of 10 K/min under an air flow of 100 ml/min. The temperature-programmed desorption of ammonia (NH_3-TPD) was carried out with an Autochem 2920

equipment (Micromeritics). The calcined samples were pretreated at 823 K for 1 h in He and then were saturated with ammonia at 373 K for 30 min. After the samples were purged with He, they were heated at 10 K/min from 373 K to 923 K.

2.3. Adsorption experiments

Adsorption isotherms of CH_4 and CO_2 on the samples were measured with a Micromeritics ASAP 2020 apparatus at 298 K and pressures up to 101 kPa. Adsorption isotherm of N_2 was performed on a Micromeritics Gemini VII 2390 device. Standard sample has been measured on both apparatus to verify the data comparability, and the same results were obtained. The adsorption temperature was controlled by ice-water or by using a Dewar bottle with a circulating jacket connected to a thermostatic bath utilizing water as the coolant. Before analysis, all samples were degassed under vacuum at 623 K for 6 h. The free space of the tube was determined with helium gas. Ultrahigh purity N_2, CH_4 and CO_2 were used for all adsorption experiments.

The Henry's law selectivity of gas component i over j at 298 K was calculated based on the following equation:

$$S_{i,j} = K_i/K_j$$

Here, K_i and K_j are the Henry's law constants for adsorption components of i and j. K_i and K_j were obtained by calculating the initial slopes of CO_2 and CH_4 isotherms.

2.4. Breakthrough experiments

The breakthrough experiment system contains a fixed adsorbent bed and bypass line for calibrating the mass spectrum of the feed gas [47]. 0.35 g of calcined sample D4 was packed between cotton plugs in a quartz tube. The packed column was initially purged with He flow (20 ml/min) and heated to 723 K for activation. The breakthrough temperature was controlled by using a circulating water thermostatic bath keeping at 298 K. Binary gas mixtures of CO_2/N_2 (20:80 v/v) and CO_2/CH_4 with a 20:80 (v/v) were allowed to pass though the sample at a flow rate of 15 ml/min until all the components reached their equilibrium concentration. Effluent gases from the packed column were monitored by a mass spectrometer. Breakthrough was defined to be 10% of the feed concentration of each gas. The retention time was calculated by subtracting the blank breakthrough time obtained with the quartz sample tube packed with only cotton from the observed breakthrough time. In the figures, breakthrough curves are shown in the form of the normalized gas ion intensities $I_i/I_{i,0}$, where I_i and $I_{i,0}$ are the in measured ion intensity of component i at the column outlet and the feed gas, respectively.

3. Results and discussion

3.1. Synthesis and characterization of SAPO-34

The XRD patterns of the as-synthesized products are shown in Fig. 1. Interestingly, SAPO-34s could be obtained in the DMEA, DEAE, DIPA, and DGA systems, while SAPO-44 and SAPO-5 crystallize from MDEA and TEOA systems, respectively. When DEA and TIPA are used as the template and solvent, only amorphous phase and tridymite with minor SAPO-5 are obtained. To the best of our knowledge, it is the first report on DIPA and DGA as the template for SAPO-34, and MDEA for SAPO-44. It should be noted that a structure distortion exists in the framework of SAPO-44 as compared with that of SAPO-34, though both possess the chabazite structure topology [48]. The major difference between them as reflected in the XRD patterns exists in the distance of two peaks

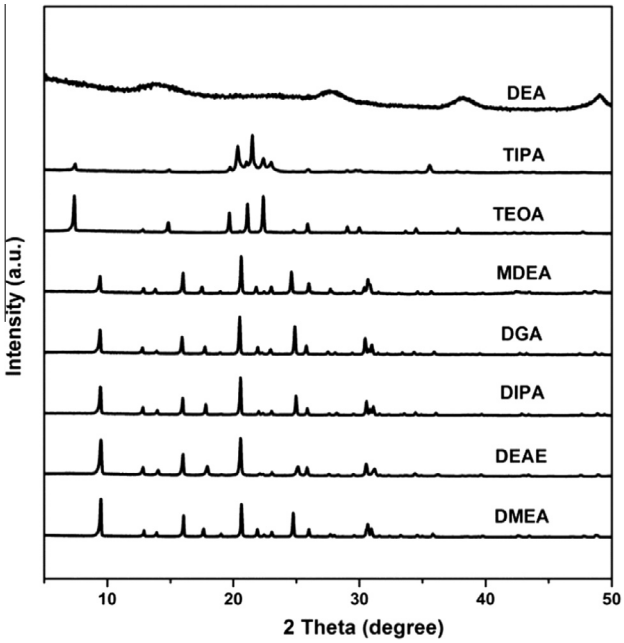

Fig. 1. Powder XRD patterns of the as-synthesized samples. All syntheses were carried out at 473 K for 48 h with starting molar ratio of 8.0 R:1.0Al_2O_3:1.0P_2O_5:0.4SiO_2:15.4H_2O (R: alkanolamine).

in the range of 23–26° (2θ) and the relative intensities of the neighboring peaks around 30° (2θ). Considering the important applications of the SAPO-34 molecular sieve in adsorption and catalysis, aminothermal syntheses of SAPO-34 with the two novel templates and their physicochemical properties are further investigated in detail.

The effect of Si amount on the synthesis of SAPO-34 with DGA and DIPA as the solvent and template is displayed in Table 1. Without Si in the initial gel, amorphous products instead of AlPO-34 are acquired. This is not surprising because AlPO-34 normally crystallized in the presence of fluoride. SAPO-34 could be obtained when the Si content is between 0.2 and 1.0. It indicates that the aminothermal synthesis offers a wide range of silicon concentration for the crystallization of SAPO-34. Further increasing the Si content leads to SAPO-34 phase but with a little amorphous silica, which suggests a upper limitation for the Si incorporation into the framework. The product compositions given in Table 1 reveal that the Si content in two series of SAPO-34s rises with its increase in the gel, though the Si incorporation degree shows a decreasing trend. The variation range of Si concentration in SAPO-34-DGA is obviously larger than that in SAPO-34-DIPA. The lowest Si amount in SAPO-34-DGA reaches 0.136 (sample D1), which is even higher than that in sample I3, suggesting that DGA has a stronger ability of inducing Si into the framework than DIPA. This is possibly related to the relatively smaller molecule size of DGA. That is, more DGA molecules than DIPA can be included in SAPO-34 crystals and thus larger amount of Si atoms are needed to be incorporated to balance the protonated amines. Similar phenomena have been reported for SAPO-34 templated by small amines such as DEA and MOR [18,22]. Moreover, hydrothermal syntheses with two amines as the template are investigated for comparison. SAPO-34 crystallized with DGA as the template (sample DH), which shows a little lower Si content than the corresponding aminothermal sample D2. SAPO-11 (sample IH1) rather than SAPO-34 is acquired when DIPA is used, suggesting that aminothermal environment has the possibility to induce special results as compared with hydrothermal method. According to the literatures, DIPA is also a novel template for the synthesis of SAPO-11 molecular sieve.

Table 1
Synthesis of SAPO molecular sieves based on DGA and DIPA systems.

Sample	Gel composition R:Al_2O_3:P_2O_5:SiO_2:H_2O[a]	$V_{amine/water}$	Product	Product composition	Relative[b] crystallinity (%)	Si[c] incorp.
D0	R = DGA 8.0:1.0:1.0:0:15.4	2.9	Amorphous			
D1	R = DGA8.0:1.0:1.0:0.2:15.4	2.9	SAPO-34+ amorphous	$Al_{0.502}P_{0.362}Si_{0.136}$	50	2.90
D2	R = DGA8.0:1.0:1.0:0.4:15.4	2.9	SAPO-34	$Al_{0.491}P_{0.355}Si_{0.154}$	100	1.69
D3	R = DGA8.0:1.0:1.0:0.75:15.4	2.9	SAPO-34	$Al_{0.472}P_{0.320}Si_{0.208}$	98	1.32
D4	R = DGA 8.0:1.0:1.0:1.0:15.4	2.9	SAPO-34	$Al_{0.460}P_{0.299}Si_{0.241}$	95	1.21
I0	R = DIPA 8.0:1.0:1.0:0:15.4	3.9	Amorphous			
I1	R = DIPA 8.0:1.0:1.0:0.2:15.4	3.9	SAPO-34	$Al_{0.503}P_{0.402}Si_{0.094}$	80	1.97
I2	R = DIPA 8.0:1.0:1.0:0.4:15.4	3.9	SAPO-34	$Al_{0.503}P_{0.395}Si_{0.102}$	91	1.12
I3	R = DIPA 8.0:1.0:1.0:1.0:20.0	3.0	SAPO-34	$Al_{0.497}P_{0.393}Si_{0.110}$	100	0.56
DH	R = DGA 3.0:1.0:1.0:0.4:50.0		SAPO-34	$Al_{0.494}P_{0.358}Si_{0.148}$		
IH1	R = DIPA 2.0:1.0:1.0:0.4:50.0		SAPO-11	$Al_{0.509}P_{0.452}Si_{0.039}$		
IH2	R = DIPA 3.0:1.0:1.0:0.4:50.0		SAPO-5+ SAPO-11			

[a] Water from each resource has been calculated into the gel composition (crystallization condition: 473 K, 48 h).
[b] The relative crystallinity is calculated based on the intensity of the three strongest peaks (2θ = 9.5, 16.0 and 20.5o) in the XRD patterns.
[c] Si incorp. = $[Si/(Si + Al + P)]_{product}/[Si/(Si + Al + P)]_{gel}$.

The SEM images of the selected samples are presented in Fig. 2. Crystals with typical rhombohedral morphology and micrometer crystal size are observed for all SAPO-34 samples. SAPO-11 shows a sphere-like morphology, which consists of small crystals. The textual properties of the samples are given in Table 2. All investigated samples except sample D1 possess large surface area and high pore volume, implying the good crystallinity of these products. The relatively small surface area and pore volume of sample D1 should be due to the existence of amorphous materials, which is also in agreement with its low relative crystallinity.

The thermal analysis results of the as-synthesized samples are given in Fig. S1†. The weight losses in the temperature range of 473–923 K due to the exothermal removal of organic templates are 18% and 20% for sample D2 and I2, respectively. After 923 K, no weight loss and thermal change occur until 1023 K, suggesting the good thermal stability of the aminothermal samples. Combining the results of XRF and thermal analysis, the average number of template per cage in two samples are calculated based on the topological structure of SAPO-34, with the results of 1.8 DGA for sample D2 and 1.0 DIPA for sample I2. These numbers are consistent with their ability to induce the Si into the framework of SAPO-34 as shown in the above synthesis section.

Table 2
Textural properties of the samples.

Sample	Surface area (m^2/g)			Pore volume (cm^3/g)	
	S_{total}[a]	S_{micro}[b]	S_{ext}[c]	V_{total}	V_{micro}[d]
D1	401	401	0	0.23	0.22
D2	538	538	0	0.28	0.27
D3	587	585	2	0.27	0.27
D4	587	587	0	0.28	0.28
I2	555	555	0	0.26	0.26

[a] BET surface area.
[b] *t*-Plot micropore surface area.
[c] *t*-Plot external surface area.
[d] *t*-Plot micropore volume.

Solid-state ^{29}Si, ^{31}P, and ^{27}Al MAS NMR spectra are measured to investigate the local atomic environments in the as-synthesized

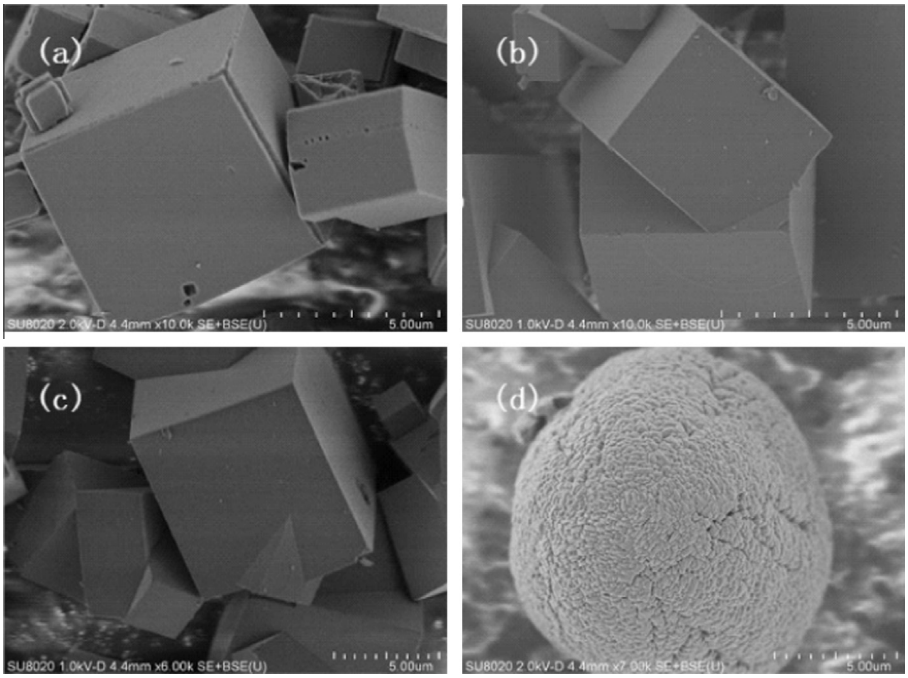

Fig. 2. SEM images of the as-synthesized samples D2 (a), D4 (b), I2 (c), and IH1 (d).

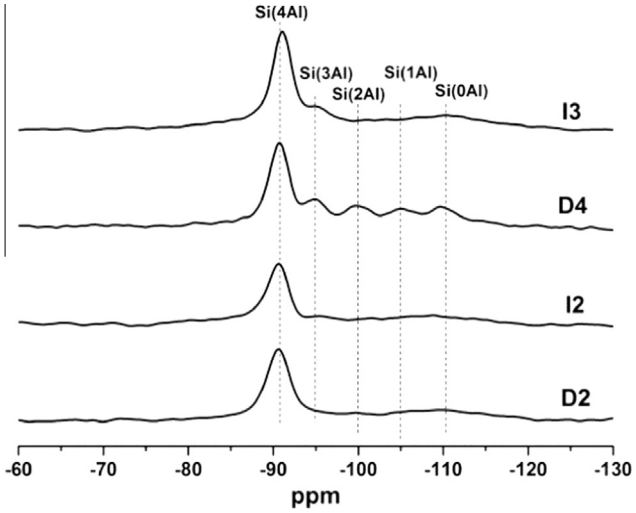

Fig. 3. ^{29}Si MAS NMR spectra of the as-synthesized samples.

samples. The ^{29}Si MAS NMR spectra are shown in Fig. 3. Only one signal at −91 ppm, ascribed to Si (4Al) environment (SM2 substitution), is observed for sample D2. One more peak with weak intensity at −94 ppm appears in the spectrum of sample I2, which is due to the Si (3Al) environment, implying the formation of Si island. Following the increase of Si concentration in the solid samples, the spectra become complex. Sample D4, which possesses the highest Si concentration, gives a spectrum with five signals at −91, −92, −93, −95, and −110 ppm, corresponding to the presence of five different Si (*n*Al) (n = 4–0) species [22]. Moreover, the content of Si islands in sample I3 is also enhanced as compared with that in sample I2, as judging from the increasing percentages of Si (3Al) and Si (0Al) species in the spectrum. It is generally accepted that the template number occluded in SAPO molecular sieves has a great effect on the Si coordination environment. In combination with the template number per CHA cage, the theoretical maximum of Si (4Al) species accommodated in the framework of SAPO-34 are calculated to be 0.150 and 0.083 for SAPO-34-DGA and SAPO-34-DIPA, respectively [25]. This explains well why only Si (4Al) appears for sample D2 even if its silicon content is as high as 0.154 (∼0.150) and different silicon environments appear for sample I2 with silicon content of only 0.10 (>0.083).

The ^{31}P MAS NMR spectra (Fig. S2†) of the four samples present strong symmetric peak at −28.1 ppm that can be assigned to P (4Al) environment, corresponding to the fact that P-O-Si linkages are nonexistent in the SAPOs. The weak resonances in the range of −15 to −20 ppm in the spectrum of sample D2 implies the existence of small amount of P species with low condensation degree [49]. The ^{27}Al MAS NMR spectra given in Fig. S3† show that samples D2 and D4 have only one peak at 38.2 ppm assigned to Al atoms in tetrahedral environment in the framework, and samples I2 and I3 show an additional resonance centered at 13.5 ppm besides the strong peak. The weak peak at 13.5 ppm may be attributed to penta-coordinated Al formed by an additional interaction of one water or template molecule to the framework aluminium [50].

3.2. Adsorption isotherms

Samples D2 and I2 are first employed as adsorbents for CO_2 and CH_4. Fig. S4† displays the adsorption isotherms of the samples acquired at 298 K with pressures up to 101 kPa. The adsorption capacities of gas molecules on adsorbents are summarized in Table 3. Clearly, both samples can adsorb much more CO_2 than CH_4, attributable to the synergic effects of the small pore apertures of adsorbents and the strong quadrupolar interactions of CO_2 with the adsorption sites. The maximum loading of CO_2 on sample D2 is higher than that on sample I2, though the adsorption selectivity ($\alpha = CO_2/CH_4$) obtained on the former is a little lower than on the latter. It is worthy to note that such a high CO_2 uptake on sample D2 (3.90 mmol/g at 298 K and 101 kPa) is not very common, which is among the highest values for CO_2 adsorption on SAPO molecular sieve sorbents. Therefore, a series of SAPO-34s-DGA with different Si contents are explored as adsorbents considering that Brønsted acid sites in SAPO materials are the preferential CO_2 adsorption sites [39,44]. The adsorption results of SAPO-34s-DGA are shown in Fig. S4† and Table 3. Interestingly, the uptakes of CO_2 rise with the increasing silicon contents in the adsorbents and sample D4 gives the highest value of 4.55 mmol/g. The adsorbed amount of CH_4 also shows an increasing trend, which thus causes a slight decline of CO_2/CH_4 selectivity from sample D1 to D4. This implies that the Si content of SAPO-34 has great influence on the CO_2 uptake, in consistence with the results of CO_2 adsorption on SAPO SAT-7 reported by Maurin et al. [45].

It should be mentioned that the relationship between acid concentration and Si content is not always straight-forward, especially when different Si species exist [51]. In order to better understand the relationship between acidic properties and CO_2 uptake, NH_3-TPD experiments of samples D1–D4 are therefore carried out. The profiles and deconvolution results are given in Fig. S5† and Table 4, respectively. It is clear that both the acid strength and acid amounts increase along with the rising Si content in SAPO-34s-DGA. Moreover, ^{1}H MAS NMR spectra of the samples are also determined to obtain the direct information of Brønsted acid concentration. As shown in Table 4, the number of Brønsted acid sites increases from sample D1 to D4, in agreement well with the results of NH_3-TPD. The acid characterization results, associated with the CO_2 adsorption results indicate that CO_2 uptakes are in line with the acid concentrations in SAPO-34. The rising initial slope in the isotherms from sample D1–D4 should be related to the increasing acid strength of the adsorbents, since CO_2 molecules preferentially interact with the most energetic adsorption sites.

To determine the CO_2/N_2 separation efficiency on sample D4, N_2 adsorption isotherm at 298 K is conducted. As shown in Table 3 and Fig. S6†, the N_2 capacity on sample D4 is only 0.27 mmol/g at 298 K and 101 kPa. Therefore, the selectivity for CO_2 over N_2 is calculated to be as high as 16.85. The superiority of sample D4 in the selectivity becomes more evident when comparing the CO_2/N_2 adsorption ratios at lower pressure ($\alpha = 52.33$ at 298 K and 10 kPa), which would be useful when the CO_2 amount to be removed is small.

Henry's Law constants of CO_2, CH_4 and N_2 at 298 K are further calculated in order to evaluate the intrinsic selectivity on sample D4, which is the upper limit of equilibrium selectivity. Details for the calculation are given in the experimental section and the initial slopes of CO_2, CH_4 and N_2 adsorption isotherms are plotted in Figs. S7† and S8†. From these data, the intrinsic selectivities of CO_2/CH_4 and CO_2/N_2 are estimated to be as high as 26:1 and 82:1, respectively.

3.3. Breakthrough experiments

From the above results, it seems feasible that SAPO-34-DGA molecular sieve with high Si content can be applied to CO_2 elimination from gas mixtures. To further evaluate the dynamic separation performance of the sample, we have carried out breakthrough experiments for separation of CO_2/CH_4 and CO_2/N_2 gas mixtures according to the methodology described by Britt et al. [52]. Fig. 4a shows the breakthrough of CO_2/N_2 mixture (20:80 v/v) on sample D4 at 298 K. N_2 breaks quickly with almost no retention on the adsorbent while CO_2 is preferentially retained until the

Table 3
Adsorption data of CO_2 and CH_4 on SAPO-34 molecular sieves at 298 K and 101 kPa.

Sample	CO_2 uptake (mmol/g)	CH_4 uptake (mmol/g)	N_2 uptake (mmol/g)	$\alpha(CO_2/CH_4)$	$\alpha(CO_2/N_2)$
D1	3.17	0.38		8.34	
D2	3.90	0.53		7.36	
D3	4.33	0.56		7.73	
D4	4.55 (5.35)[a]	0.64	0.27	7.11	16.85
I2	3.41	0.45		7.58	

[a] The value in parentheses represent the CO_2 uptake at 273 K and 101 kPa.

Table 4
Results of acid amounts on SAPO-34 samples from NH_3-TPD and ^1H MAS NMR.

Sample	Weak acid sites		Moderate acid sites		Strong acid sites		Total (%)	Acid amount (mmol/g)[a]
	T (K)	Percentage	*T* (K)	Percentage	*T* (K)	Percentage		
D1	502	8.76	651	24.33	740	24.21	57.3	1.67
D2	493	15.29	676	38.54	750	22.17	76.0	2.08
D3	494	14.30	660	38.74	753	40.36	93.4	2.24
D4	493	13.99	674	50.07	761	35.94	100.0	2.40

[a] Obtained from ^1H MAS NMR.

adsorbent is saturated. Fig. 4b presents the breakthrough curves of CO_2/CH_4 (20:80 v/v). CH_4 also breaks up quickly as expected, suggesting that the SAPO-34 sample does not adsorb CH_4 significantly.

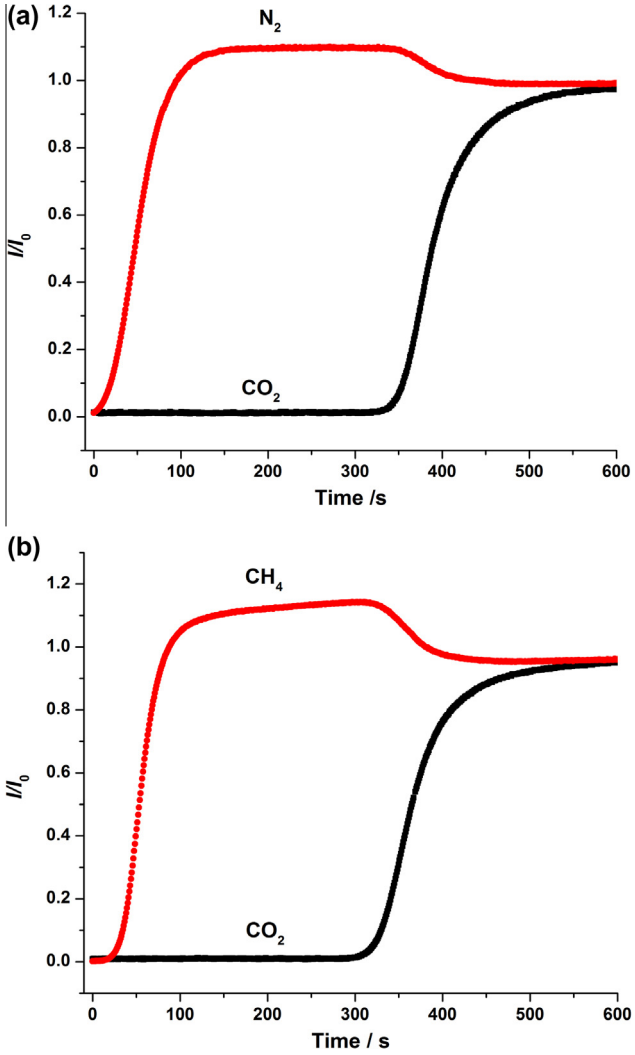

Fig. 4. Breakthrough curves corresponding to the separation of CO_2/N_2 (20:80 v/v) and CO_2/CH_4 (20:80 v/v) gas mixtures on sample D4 at 298 K and 101 kPa.

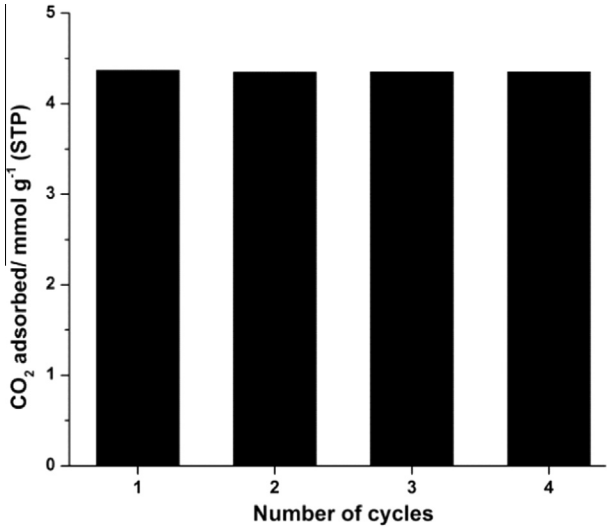

Fig. 5. The cycle capacity of CO_2 on SAPO-34-DGA (sample D4) at 298 K and 101 kPa.

Based on the breakthrough data, the dynamic adsorption capacity of CO_2 before breakthrough is calculated to be 8.26 wt% and 8.2 wt% for CO_2/N_2 and CO_2/CH_4 mixtures respectively.

The regeneration property is an important feature of the adsorbent because the energy required for CO_2 release has a great effect on the cost of the PSA processes. Consequently, the cycle capacity of sample D4 is examined by isotherm adsorption experiments at 298 K for four times. The sample was regenerated at near-vacuum conditions at room temperature for an hour without heating before the next-round adsorption. The results are displayed in Fig. 5. No significant change in the CO_2 uptake on sample D4 is observed even after four cycles, indicating the facile regeneration of the adsorbent at mild conditions. These results suggest that SAPO-34-DGA (sample D4) could be employed as an efficient adsorbent with large dynamic CO_2 uptake and easy regeneration ability.

4. Conclusions

The present work demonstrates that alkanolamines could be used as the solvent and template to conduct aminothermal

synthesis of SAPO molecular sieves. Two amines DGA and DIPA are found to be the novel templates for the synthesis of SAPO-34, and MEDA for SAPO-44. Moreover, SAPO-11 is obtained for the first time with DIPA as the template under hydrothermal conditions. The Si/(Si + Al + P) ratio in SAPO-34-DGA could be tunable in a relatively wide range, whereas for SAPO-34-DIPA the Si/(Si + Al + P) ratio is limited within a very narrow range. More DGA molecules than DIPA are occluded in SAPO-34 crystals, which thus lead to a higher Si incorporation and larger Si (4Al) concentration in SAPO-34-DGA. The CO_2 uptakes are found to be in line with the acid concentrations of SAPO-34 adsorbents. Breakthrough experiments confirm that the SAPO-34-DGA (sample D4) has excellent property of dynamic preferential adsorption of CO_2 from both CO_2/N_2 and CO_2/CH_4 mixtures with a capacity of ~8.2 wt%. Moreover, the CO_2 adsorption capacity of SAPO-34-DGA is reversible with no significant changes under mild regeneration conditions. All of the features suggest the potential of sample D4 as efficient adsorbent for the removal of CO_2 from natural gas or flue gas.

Acknowledgements

We are grateful for the financial support from the National Natural Science Foundation of China (NSFC 21101150).

Appendix A. Supplementary data

Supplementary data associated with this article can be found, in the online version, at http://dx.doi.org/10.1016/j.micromeso.2014.03.028.

References

[1] M.E. Davis, Nature 417 (2002) 813–821.
[2] A. Corma, Chem. Rev. 979 (1997) 2373–2419.
[3] J.F.M. Denayer, L.I. Devriese, S. Couck, R. Singh, P.A. Webley, G.V. Baron, J. Phys. Chem. C 112 (2008) 16593–16599.
[4] Database of Zeolite Structures. http://www.iza-structure.org/databases/.
[5] R.E. Morris, S. Weigel, J. Chem. Soc. Rev. 26 (1997) 309–317.
[6] B.M. Lok, C.A. Messina, R.L. Patton, R.T. Gajek, T.R. Cannan, E.M. Flanigen, J. Am. Chem. Soc. 106 (1984) 6092–6093.
[7] C.A.M. B. Lok, M.R.L. Patton, R.T. Gajek, T.R. Cannan, E.M. Flanigen, U.S. Patent 4,440,871, 1984.
[8] J. Liang, Appl. Catal. 64 (1990) 31–40.
[9] S. Wilson, P. Barger, Micropor. Mesopor. Mater. 29 (1999) 117–126.
[10] S.S.A. Talesh, S. Fatemi, S.J. Hashemi, M. Ghasemi, Sep. Sci. Technol. 45 (2010) 1295–1301.
[11] M.A. Carreon, S. Li, J.L. Falconer, R.D. Noble, J. Am. Chem. Soc. 130 (2008) 5412–5413.
[12] Y.Y. Tian, L.L. Fan, Z.Y. Wang, S.L. Qiu, G.S. Zhu, J. Mater. Chem. 19 (2009) 7698–7703.
[13] D. Fan, P. Tian, S.T. Xu, Q.H. Xia, X. Su, L. Zhang, Y. Zhang, Y.L. He, Z.M. Liu, J. Mater. Chem. 22 (2012) 6568–6574.
[14] D. Fan, P. Tian, X. Su, Y.Y. Yuan, D.H. Wang, C. Wang, M. Yang, L.Y. Wang, S.T. Xu, Z.M. Liu, J. Mater. Chem. A. 1 (2013) 14206–14213.
[15] Y. Hirota, K. Murata, S. Tanaka, N. Nishiyama, Y. Egashira, K. Ueyama, Mater. Chem. Phys. 123 (2010) 507–509.
[16] Y.Y. Jin, Q. Sun, G.D. Qi, C.J. Yang, J. Xu, F. Chen, X.J. Meng, F. Deng, F.S. Xiao, Angew. Chem. Int. Ed. 52 (2013) 1–5.
[17] N. Nishiyama, M. Kawaguchi, Y. Hirota, D.V. Vu, Y. Egashira, K. Ueyama, Appl. Catal. A 362 (2009) 193–199.
[18] A.M. Prakash, S. Unnikrishnan, J. Chem. Soc., Faraday Trans. 90 (1994) 2291–2296.
[19] E. Dumitriu, A. Azzouz, V. Hulea, D. Lutic, H. Kessler, Micropor. Mater. 10 (1997) 1–12.
[20] B.M. Lok, C.A. Messina, R.L. Patton, R.T. Gajek, T.R. Cannan, E.M. Flanigen, U.S. Patent 4,440,871, 1984.
[21] Y.X. Wei, D.Z. Zhang, Z.M. Liu, B.L. Su, J. Catal. 238 (2006) 46–57.
[22] G.Y. Liu, P. Tian, J.Z. Li, D.Z. Zhang, F. Zhou, Z.M. Liu, Micropor. Mesopor. Mater. 111 (2008) 143–149.
[23] L.P. Ye, F.H. Cao, W.Y. Ying, D.Y. Fang, Q.W. Sun, J. Porous Mater. 18 (2011) 225–232.
[24] R. Vomscheid, M. Briend, M.J. Peltre, P.P. Man, D. Barthomeuf, J. Phys. Chem. 98 (1994) 9614–9618.
[25] D. Barthomeuf, J. Phys. Chem. 97 (1993) 10092–10096.
[26] C.S. Song, Catal. Today 115 (2006) 2–32.
[27] H.Q. Yang, Z.H. Xu, M.H. Fan, R. Gupta, R.B. Slimane, A.E. Bland, I. Wright, J. Environ. Sci. 20 (2008) 14–27.
[28] S. Li, J.G. Martinek, J.L. Falconer, R.D. Noble, T.Q. Gardner, Ind. Eng. Chem. Res. 44 (2005) 3220–3228.
[29] O. Bolland, S. Saether, Energy Convers. Manage. 33 (1992) 467–475.
[30] A.P. Veawab, P. Tontiwachwuthikul, A. Chakma, Ind. Eng. Chem. Res. 38 (1999) 3917–3924.
[31] M. Palomino, A. Corma, F. Rey, S. Valencia, Langmuir 26 (2010) 1910–1917.
[32] D. Bonenfant, M. Kharoune, P. Niquette, M. Mimeault, R. Hausler, Sci. Technol. Adv. Mater. 9 (2008) 013007.
[33] M. Palomino, A. Corma, J.L. Jordá, F. Rey, S. Valencia, Chem. Commun. 48 (2012) 215–217.
[34] Q.L. Liu, T. Pham, M.D. Porosoff, R.F. Lobo, ChemSusChem 5 (2012) 2237–2242.
[35] M. Moliner, C. Martínez, A. Corma, Chem. Mater. (2013), http://dx.doi.org/10.1021/cm4015095.
[36] M.R. Hudson, W.L. Queen, J.A. Mason, D.W. Fickel, R.F. Lobo, C.M. Brown, J. Am. Chem. Soc. 134 (2012) 1970–1973.
[37] F.N. Ridha, Y.X. Yang, P.A. Webley, Micropor. Mesopor. Mater. 117 (2009) 497–507.
[38] M.M. Lozinska, E. Mangano, J.P.S. Mowat, A.M. Shepherd, R.F. Howe, S.P. Thompson, J.E. Parker, S. Brandani, P.A. Wright, J. Am. Chem. Soc. 134 (2012) 17628–17642.
[39] O. Cheung, Q. Liu, Z. Bacsik, N. Hedin, Micropor. Mesopor. Mater. 156 (2012) 90–96.
[40] T. Takeguchi, W. Tanakulrungsand, T. Inui, Gas Sep. Purif. 7 (1993) 3–9.
[41] S.J. Li, J.L. Falconer, R.D. Noble, Adv. Mater. 18 (2006) 2601–2603.
[42] A.G. Arévalo-Hidalgo, J.A. Santana, R.Q. Fu, Y. Ishikawa, A.J. Hernández-Maldonado, Micropor. Mesopor. Mater. 130 (2010) 142–153.
[43] S.R. Venna, M.A. Carreon, Langmuir 27 (2011) 2888–2894.
[44] I. Deroche, L. Gaberova, G. Maurin, P. Llewellyn, M. Castro, P. Wright, Adsorption 14 (2008) 207–213.
[45] I. Deroche, L. Gaberova, G. Maurin, M. Castro, P.A. Wright, P.L. Llewellyn, J. Phys. Chem. C 112 (2008) 5048–5056.
[46] L. Chen, S.Y. Zhu, H.M. Wang, Y.M. Wang, Solid State Sci. 13 (2011) 2024–2029.
[47] X. Su, P. Tian, D. Fan, Q.H. Xia, Y. Yang, S.T. Xu, L. Zhang, Y. Zhang, D.H. Wang, Z.M. Liu, ChemSusChem 6 (2013) 911–918.
[48] S. Ashtekar, S.V.V. Chilukuri, D.K. Chakrabarty, J. Phys. Chem. 98 (1994) 4878–4883.
[49] R.F. Mortlock, A.T. Bell, C.J. Radke, J. Phys. Chem. 97 (1993) 767–774.
[50] C. Yannoni, Acc. Chem. Res. 15 (1982) 201–208.
[51] P. Mériaudeau, V.A. Tuan, F. Lefebvre, Vu T. Nghiem, C. Naccache, Micropor. Mesopor. Mater. 26 (1998) 161–173.
[52] D. Britt, H. Furukawa, B. Wang, T.G. Glover, O.M. Yaghi, PNAS 106 (2009) 20637–20640.